Applied Catalysis A: General 469 (2014) 328–339

Contents lists available at ScienceDirect

Applied Catalysis A: General

journal homepage: www.elsevier.com/locate/apcata

Hydroconversion of *n*-hexadecane on Pt/silica-alumina catalysts: Effect of metal loading and support acidity on bifunctional and hydrogenolytic activity

Francesco Regali[a,*], Leonarda Francesca Liotta[b], Anna Maria Venezia[b], Magali Boutonnet[a], Sven Järås[a]

[a] KTH Royal Institute of Technology, School of Chemical Science and Engineering, Department of Chemical Engineering and Technology, Teknikringen 42, 10044 Stockholm, Sweden
[b] Istituto per lo Studio dei Materiali Nanostrutturati, ISMN-CNR, Palermo, Italy

ARTICLE INFO

Article history:
Received 18 June 2013
Received in revised form
23 September 2013
Accepted 26 September 2013
Available online 6 October 2013

Keywords:
Bifunctional hydrocracking
Hexadecane
Hydroconversion
Hydrogenolysis
Platinum
Silica–alumina

ABSTRACT

Bifunctional catalysts based on platinum and amorphous silica–alumina were studied in the hydroconversion of *n*-hexadecane. The influence of platinum loading and support acidity on activity and selectivity were assessed. The contribution of hydrogenolysis reactions on top of bifunctional hydrocracking was shown to depend not only on metal loading, but also on the effect of support acidity on the intrinsic activity of the platinum sites. The yield of cracking products, and their linear alkane fraction, increased with metal loading, while the isomerization yield was practically independent of the metal content. On a support of high Brønsted acidity, the rate of formation of methane was proportional to the platinum surface area, indicating that demethylation occurred by metal-catalyzed hydrogenolysis. On the other hand, the methane site-time yield was one order of magnitude lower on a catalyst with negligible Brønsted acidity. Pt-catalyzed hydrogenolysis was also investigated during selective poisoning of acid sites by co-feeding pyridine and comparing the effect of hydrogen partial pressure on reaction rates. In the presence of pyridine, total hydroconversion activity was reduced by one order of magnitude while rates to methane and linear cracking products remained relatively high. These observations indicate that acid sites do not intervene in the mechanism, but that support acidity affects the hydrogenolytic activity of platinum sites.

1. Introduction

Hydroconversion of linear alkanes on bifunctional catalysts has been thoroughly studied. The commonly accepted classical bifunctional hydrocracking mechanism [1–3] states that alkanes are converted by dehydrogenation/hydrogenation on metal sites and carbenium ion chemistry on acid sites: The alkane molecule is first dehydrogenated on a metal site to a corresponding alkene; then the alkene diffuses to a Brønsted acid site where it is protonated to a carbenium ion. This carbocation undergoes skeletal isomerization and cracking, the products of which are desorbed as alkenes which are finally hydrogenated back to alkanes on metal sites. At certain conditions of operating parameters and relative strength and concentration of metal and acid sites (functional balance), the metal-catalyzed dehydrogenation and hydrogenation reactions are at quasi-equilibrium, and the overall reaction rate is controlled by the acid-catalyzed isomerization and cracking reactions. When this occurs, hydrocracking is defined as ideal [3,4]. Although this mechanism has gained widespread acceptance, some details are still debated, in particular as regards the function responsible for the activation of the alkane molecules and the role of the diffusion of alkene intermediates to the metal sites [5,6].

Acidic supports used in combination with noble metals in hydroconversion processes range from chlorinated aluminas, zeolites, amorphous silica–aluminas, to silicas or aluminas, in order of decreasing acidity. Common noble metals such as platinum and palladium are active, to different extents and depending on size and morphology of the metal particles, for dehydrogenation, hydrogenation, isomerization and hydrogenolysis [7,8]. When the metal and acid functions are combined in bifunctional hydroconversion, synergic effects can be observed and the resulting combination cannot be predicted by the activities of the two functions alone [2]. Moreover, the catalytic activity and specificity of the metal particles are affected by their interaction with the support [9,10]; likewise, the acid function of the support is prone to be modified by the presence of metal crystallites [11]. This situation generates

* Corresponding author. Tel.: +46 8 790 8243.
E-mail address: regali@kth.se (F. Regali).

0926-860X/$ – see front matter © 2013 Elsevier B.V. All rights reserved.
http://dx.doi.org/10.1016/j.apcata.2013.09.048

a high complexity in the reactivity patterns occurring on this kind of bifunctional catalysts. The major parameter affecting product selectivities is the metal–acid site balance, which is determined by the strength distribution and concentration of acid sites as well as the activity, concentration and properties of metal sites.

The effect of metal–acid site ratio on hydrocracking/hydroisomerization of paraffins has been the subject of many studies, typically using platinum on zeolite-based catalysts, in which strong acidity is balanced by a strong hydrogenation function. The most important findings were related to the achievement of "ideality" and its effect on observed reaction patterns and selectivity [12–17]. Catalyst systems using platinum supported on milder acids, such as silica–aluminas, are used for the hydroconversion of long chain paraffins when the desired products are middle distillate fuels [18–21]. In such systems, metal-catalyzed hydrogenolysis is likely to occur alongside bifunctional hydrocracking. This additional mechanism leads to a shift in selectivity toward linear alkanes and to the formation of methane and ethane, unwanted products which are not formed by purely bifunctional hydrocracking. Ribeiro et al. studied hydroisomerization of *n*-hexane on Pt/Y-zeolites and observed C_1 and C_2 formation on large metal surface area catalysts [15]. Calemma et al. observed the formation of direct cracking products on a Pt/silica-alumina catalyst, presumably formed by the hydrogenolytic pathway, in the hydrocracking of long chain paraffins [22]. Blomsma et al. reported on an added hydrogenolysis contribution of platinum on H-Beta zeolite catalysts in the hydrocracking of *n*-heptane [23]; Böhringer et al. summarized the effects of non-selective hydrogenolysis and methanolysis on the observed distribution of cracking products from the hydrocracking of *n*-tetradecane [24]. However, a more detailed analysis to assess the extent of this superimposed metal-catalyzed mechanism at varying metal–acid site ratios has, to our best knowledge, not been published.

The purpose of this work is therefore to investigate the relationship between the two catalytic functions in the hydroconversion of *n*-hexadecane using a metal with high hydrogenating activity (Pt) supported on a material of mild Brønsted acidity (silica–alumina). This study addresses the influence of platinum loading on total hydroconversion activity and on product distribution. Particular consideration is given to the selectivity toward methane and the degree of isomerization of the cracking products with varying platinum loading. In order to isolate the contribution of the monofunctional metal-catalyzed hydrogenolysis mechanism a dual approach was used: (1) a catalyst using a support with negligible Brønsted acidity was tested; (2) selective poisoning of acid sites by co-feeding pyridine was performed on one of the Pt/silica-alumina catalysts. The influence of hydrogen partial pressure on the rates to different products was studied in presence and in absence of pyridine.

2. Experimental

2.1. Catalyst preparation

The silica–alumina supports, Siral 40 (40-wt% SiO_2, 60-wt% Al_2O_3) and Siral 1 (1-wt% SiO_2, 99-wt% Al_2O_3) were obtained from Sasol Germany GmbH. The supports were sieved to the desired size (90–200 μm), dried at 120 °C for 6 h and subsequently calcined in air at 500 °C for 2 h, increasing the temperature with a heating rate of 2 °C/min. Platinum was deposited by incipient wetness impregnation, using volumes of aqueous solutions corresponding to the total pore volume of the materials, containing the appropriate amounts of tetraammineplatinum nitrate ($[Pt(NH_3)_4](NO_3)_2$, Sigma-Aldrich) to achieve the desired weight loadings. After impregnation, the materials were dried at 120 °C for 6 h, and then calcined in air at 500 °C for 4 h (heating rate 2 °C/min).

The catalysts prepared are shown in Table 1. Four different platinum weight loadings were used on Siral 40: 0.06%, 0.33%, 0.6%, 1.2%. Additionally, a catalyst containing 0.33-wt% platinum was prepared using the low acidic support Siral 1.

2.2. Catalyst characterization

Surface area and porosity were determined by nitrogen adsorption using a Micromeritics ASAP 2000 unit. Before the analysis, the samples were degassed by evacuation at 250 °C for a minimum of 4 h.

Metal dispersion, crystallite size and metal surface area were measured by hydrogen chemisorption at 35 °C in a Micromeritics ASAP 2020C unit. Before each measurement 0.2–0.4 g of dried catalyst powder was evacuated at 250 °C for 4 h, cooled to 100 °C and subsequently reduced in flowing hydrogen raising the temperature to 400 °C with a heating rate of 5 °C/min and keeping the final temperature for 2 h. The sample was then evacuated and cooled to the analysis temperature. For each sample two adsorption isotherms were obtained in the pressure range from 50 to 500 mmHg, with an evacuation step in between. The chemisorptive hydrogen uptake was estimated from the difference between the two isotherms extrapolated to zero pressure. Dispersion and average particle size were calculated assuming a stoichiometry of adsorption of 1 hydrogen atom per platinum atom.

The acidic properties of the support materials and the catalysts were determined by temperature-programed desorption of ammonia (NH_3-TPD) and by FTIR spectroscopy of adsorbed pyridine.

NH_3-TPD experiments were carried out using a Micromeritics Autochem 2910 apparatus equipped with a thermal conductivity detector (TCD) and a mass quadrupole spectrometer (Thermostar, Balzers). For each measure, a sample amount of 0.15 g was pretreated in helium at 500 °C with a heating rate of 10 °C/min and holding the final temperature for 30 min. After cooling to room temperature, ammonia was adsorbed by admitting a flow of 5% NH_3/He (30 ml/min) for 1 h. In order to remove all the physically adsorbed ammonia, the sample was purged by flowing helium (100 ml/min) at 100 °C for 1 h. Subsequently, after cooling to room temperature, ammonia desorption was started by flowing helium (30 ml/min) and heating to 500 °C with a rate of 10 °C/min. The final temperature was held for 30 min. The NH_3 desorption curves were evaluated by QMS analysis of the NH_3 fragmentation signals at mass 17, 16 and 15. A blank test at the same experimental conditions, by flowing pure He, was carried out in order to exclude that H_2O, CO_2 or

Table 1
Physical properties of the catalysts (after calcination at 500 °C for 4 h).

Catalyst	Pt loading (wt%)	BET surface area (m^2/g)	BJH adsorption pore volume (cm^3/g)	BJH ads. average pore diameter (nm)
Siral 40	0	440	0.92	8.5
Pt0.06/Siral 40	0.06	394	0.92	8.9
Pt0.33/Siral 40	0.33	387	0.94	9.1
Pt0.6/Siral 40	0.60	402	0.93	8.9
Pt1.2/Siral 40	1.20	397	0.92	9.0
Siral 1	0	227	0.62	8.8
Pt0.33/Siral 1	0.33	223	0.61	8.9

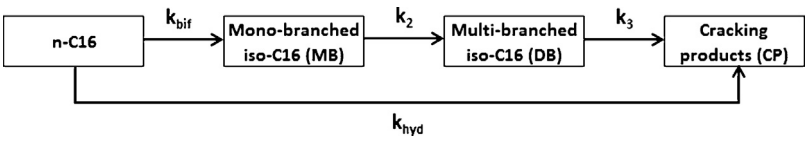

Fig. 1. Simplified reaction network.

any other impurity may affect the NH_3 adsorption and desorption processes.

Pyridine adsorption FTIR measurements were performed in an ATI Mattson FTIR spectrometer. Approximately 0.20 g of sample was pressed into a self-supporting thin wafer and placed in the FTIR cell. The sample was pretreated in high vacuum ($\sim 10^{-5}$ mmHg) at 450 °C for 1 h. The temperature was then lowered to 100 °C and a background spectrum was recorded. Pyridine was adsorbed on the sample at its ambient vapor pressure in flowing helium at 100 °C for 30 min. Spectra of adsorbed pyridine were recorded at 100 °C for 50 min; three measures were performed, after evacuation for 1 h at 150, 250 and 350 °C, respectively. Spectral bands at 1545 cm^{-1} (Brønsted) and 1450 cm^{-1} (Lewis) were considered for the estimation of acid site concentrations, using the molar extinction coefficients calculated by Emeis: 1.67 for the 1545 cm^{-1} band and 2.22 for the 1450 cm^{-1} band [25].

2.3. Catalytic testing

Hydroconversion of *n*-hexadecane (>99%, for synthesis, Merck 820633) was performed in a stainless steel tubular reactor, allowing operation up to a pressure of 80 bar. The reaction and analysis system has been described in detail elsewhere [26]. Briefly, the *n*-hexadecane liquid feed was supplied by means of a HPLC pump, and mixed with hydrogen prior to entering the reactor, which operated in co-current downflow mode. The reaction products were separated in a gas–liquid separator at room temperature. The product gas was sent, through a downstream pressure control valve, to an on-line gas chromatograph equipped with an Alumina PLOT column. The liquid products were sampled and analyzed off-line with an HP-5 column.

Before each experiment, approximately 3 g of catalyst, previously sieved to a particle size of 90–200 μm and dried overnight, was loaded into the reactor. The catalyst was activated in situ in hydrogen flow (50 N ml/min/g_{cat}) at 400 °C for 2 h, by raising the temperature with a heating ramp of 5 °C/min. Thereafter the system was pressurized in hydrogen and stabilized at the desired reaction temperature and pressure. The conditions used were T = 310 °C, P = 30 bar, $H_2/n\text{-}C_{16}H_{34}$ inlet ratio = 10 mol/mol. The total conversion of *n*-hexadecane was varied by varying the weight hourly space velocity (WHSV) between 0.25 and 18 h^{-1}. Under these conditions the distribution of cracking products was practically symmetric throughout the full conversion range, i.e. overcracking was avoided. Conversion of *n*-hexadecane is defined as $1 - F_{n\text{-C16,out}}/F_{n\text{-C16,in}}$ where F is the molar flow. The hydroconversion activity is reported as the pseudo-first-order reaction rate constant for the disappearance of *n*-hexadecane, calculated assuming plug flow behavior. Selectivities are reported on a carbon atom basis, as moles of C in product per mole of C of converted *n*-hexadecane. The products of *n*-hexadecane hydroisomerization/hydrocracking were grouped into three main lumps: mono-branched hexadecanes (MB), di- or multi-branched hexadecanes (DB), and cracking products (CP). The contributions of the two possible routes of formation of cracking products, i.e. bifunctional and hydrogenolytic, were estimated by the simple reaction network model depicted in Fig. 1. In this scheme, all reaction steps were considered first-order and irreversible [22,26]. The equations describing the concentrations profiles of the different product lumps as functions of the contact time τ (or the inverse of WHSV) are reported below.

$$C_{n\text{-C16}} = C_{n\text{-C16}_0} e^{-(k_{bif}+k_{hyd})\tau}$$

$$C_{MB} = \frac{-k_{bif} C_{n\text{-C16}_0} (e^{-k_{bif}\tau} - e^{-k_2\tau})}{k_{bif} - k_2}$$

$$C_{DB} = \frac{C_{n\text{-C16}_0} k_{bif} k_2 e^{-k_3\tau}}{(k_{bif} - k_3)(k_2 - k_3)} - \frac{C_{n\text{-C16}_0} k_{bif} k_2 (k_{bif} e^{-k_2\tau} - k_2 e^{-k_{bif}\tau} + k_3 e^{-k_{bif}\tau} - k_3 e^{-k_2\tau})}{(k_{bif} - k_2)(k_{bif} - k_3)(k_2 - k_3)}$$

$$C_{CP} = C_{n\text{-C16}_0} - C_{n\text{-C16}} - C_{MB} - C_{DB}$$

Selectivity/conversion curves for the different product lumps were obtained by non-linear regression of the experimental data. First-order rate constants are given as k_{bif} (bifunctional) and k_{hyd} (hydrogenolysis), respectively.

The effect of H_2 partial pressure was studied on a stable 1.2-wt% Pt/Siral 40 catalyst. Experiments were performed at constant *n*-hexadecane WHSV (18 h^{-1}) and total pressure (30 bar), replacing a part of the hydrogen feed with helium. The degree of vaporization of *n*-hexadecane was considered to calculate hydrogen partial pressure, which varied between 17.4 and 29.2 bar. The same set of experimental points was repeated in the presence of pyridine, mixed with *n*-hexadecane (0.8 wt%) in the feed vessel. The system was run at the reference conditions until catalytic activity reached steady state. Experimental points at reference conditions were repeated to ensure that no further deactivation occurred during the experiments with varying hydrogen partial pressure. Apparent reaction orders with respect to hydrogen were calculated by linearization of the bi-logarithmic plot of reaction rates versus inlet hydrogen pressure. Rates were approximated with space–time yields, not considering the change in composition along the reactor.

3. Results

3.1. Catalyst characterization

The textural properties of the catalysts are presented in Table 1. Addition of platinum on the Siral 40 material caused a slight decrease of surface area (~10%), but no significant differences were observed for varying platinum loading. The porous structure remained practically unaffected. On Siral 1, characterized by a smaller surface area compared to the Siral 40 (227 m^2/g vs. 440 m^2/g), the effect of 0.33-wt% platinum was negligible.

Hydrogen-chemisorption analyses (Table 2) showed that platinum particles were well dispersed on all catalysts, with dispersion values ranging from 120% to 61%, with dispersion decreasing as platinum loading increased. Values of dispersion higher than 100% are of course physically impossible, and are due to the assumption of a constant hydrogen adsorption stoichiometry coefficient equal to 1. It has been shown that adsorption stoichiometry on

Table 2
H_2-chemisorption properties of the catalysts (after calcination at 500 °C for 4 h and activation in H_2 at 400 °C for 2 h). The data are calculated from the measured chemisorption uptake assuming spherical particles and monolayer adsorption of H_2 with a stoichiometry (H/M) of 1 hydrogen atom per exposed Pt atom.

Catalyst	Pt loading (wt%)	H_2 uptake at 35 °C (cm^3 STP/g cat)	Pt dispersion (%)	Pt particle size (d_p) (nm)	Pt surface area (m^2/g_{cat})
Siral 40	0	0	–	–	–
Pt0.06/Siral 40	0.06	0.041	120[a]	0.9	0.177
Pt0.33/Siral 40	0.33	0.172	91	1.2	0.739
Pt0.6/Siral 40	0.60	0.308	89	1.3	1.325
Pt1.2/Siral 40	1.20	0.423	61	1.8	1.818
Pt0.33/Siral 1	0.33	0.151	80	1.4	0.649

[a] A value higher than 100% is probably due to an adsorption stoichiometry (H/M) exceeding unity on the smallest Pt particles.

highly dispersed noble metal catalysts depends on the size and shape of the metal clusters; the hydrogen to metal (H/M) coefficient increases due to the lower coordination number of the metal atoms in smaller particles, which causes multiple adsorption on edges and corners [27]. For the purpose of this work a comparative measure of platinum sites was needed; metal surface area was therefore used, which is proportional to the hydrogen uptake through the assumed stoichiometry factor and the cross sectional area of a Pt atom. Values of dispersion and average metal particles sizes are reported for comparison only and should not be taken as absolute measurements.

Acidic properties of the materials have been investigated using pyridine adsorption FTIR and NH_3-TPD. In this study, Siral 40, exhibiting the highest Brønsted acidity of the Siral series, and Siral 1, with very low Brønsted acidity, were used. Many authors have reported before on the acidity of these materials [28–31], especially as regards the different contents of silica and alumina. Not much work has been done about the effect of platinum addition; moreover, there seems to be disagreement in the literature about how Pt affects acidity. Leckel [19] observed a dramatic decrease in the concentration of Brønsted acid sites of a Siral 40 support after loading with 0.3-wt% of platinum, while the same amount of platinum induced Brønsted acidity on a Siral 75 support which showed no Brønsted acidity prior to metal addition. Larson et al. [11] reported on the influence of Pt on ammonia adsorption properties of a silica–alumina. Higher acidity was observed at Pt contents between 0.13 and 2.86-wt%, with a maximum increase of approximately 50% over the non-loaded support at a Pt loading of 0.53-wt%. According to Peeters et al. [29], no significant modification was induced by addition of 1.1-wt% Pt on Siral 40 and similar materials. The results of acidity measurements by pyridine adsorption FTIR are presented in Table 3. The Brønsted acidity of Siral 1 was indeed negligible and no Brønsted acidity was induced by the incorporation of 0.33-wt% platinum on this material. The concentration of Lewis acid sites (LAS) of all strengths was lower after the addition of platinum.

On Siral 40, the incorporation of platinum caused an increase in both Brønsted and Lewis acidity. The strongest Brønsted sites (BAS), measured after desorption of pyridine at 350 °C, were removed after the introduction of platinum, while the concentration of BAS of lower strength increased at all loadings, peaking for the sample containing 0.6-wt% of Pt. A similar pattern was observed for Lewis acidity, with the difference that the medium-strength LAS were slightly detrimentally affected by the presence of platinum. These measurements were confirmed by the analysis of the TPD spectra of ammonia, shown in Fig. 2 as ion current signal at mass 17. Although ammonia desorption techniques cannot distinguish between BAS and LAS, the same general trend of modification of the acidity of Siral 40 by the addition of platinum was observed. The concentration of low strength acid sites (ammonia desorption temperature <250 °C) increased at all Pt loadings, while medium strength acidity (250–400 °C) was higher for the samples containing middle levels of Pt and lower for the lowest (0.06-wt%) and highest (1.2-wt%) Pt content (cfr. LAS at 250 °C in Table 3). The concentration of the strongest acid sites, releasing adsorbed ammonia at temperatures above 400 °C, was decisively higher for the unloaded Siral 40.

Analyzing the causes behind these observed modifications in acidity is outside the scope of this work. However, some considerations can be made: Platinum crystallites supported on acidic substrates are known to assume a lower electron density, due to charge transfer to the support [32,33]; they can therefore accept electron pairs, acting as Lewis acids. Kubička et al. [34] observed a similar influence on the acid properties of zeolites following impregnation by 2-wt% Pt. They concluded that the increase in the total measured amount of Lewis acidity, and especially of the lower strength LAS, could be due to the interaction of the electron-deficient Pt crystallites with pyridine. The authors ruled out the effect of the impregnation procedure and the subsequent thermal treatment on the surface structure of the solid acids, and interpreted the changes in acid site distribution as arising from electronic interactions between metal crystallites and the surface atoms of the support [34]. Santi et al. [35] suggested also that charge transfer between the metal particles and the framework oxygen atoms was responsible for the modification of the strength of the Brønsted sites associated with bridging hydroxyl groups.

3.2. Hydroconversion of n-hexadecane

3.2.1. Bifunctional and hydrogenolytic hydrocracking activity

The linearized form of the mass balance equation for a plug flow reactor relates *n*-hexadecane conversion (χ) to space velocity (WHSV) through the pseudo-first-order rate constant (k): $-\ln(1-\chi) = k/\mathrm{WHSV}$. The rate constants were calculated from experimental data at different flow conditions. Table 4 shows the mean k values and their linear fitting parameters. The values of the intercept are close to 0 and R^2 values are very close to unity, indicating a high goodness of fit for the first-order reaction model. It is directly apparent that the catalyst supported on Siral 1 is much less

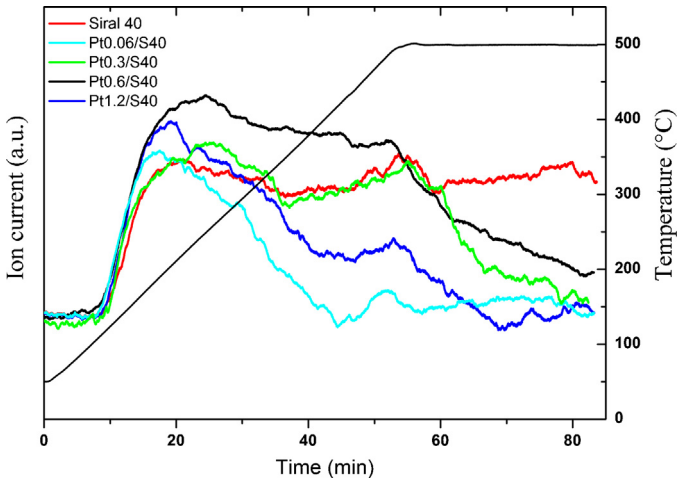

Fig. 2. NH_3-TPD profiles of the Pt/Siral 40 catalysts.

Table 3
Acid properties of the catalysts (after calcination at 500 °C for 4 h).

Catalyst	Pt loading (wt%)	Brønsted acid sites			Lewis acid sites		
		150 °C	250 °C	350 °C	150 °C	250 °C	350 °C
		(μmol/g)			(μmol/g)		
Siral 40	0	44	31	4	114	54	12
Pt0.06/Siral 40	0.06	54	38	0	136	43	0
Pt0.33/Siral 40	0.33	59	43	0	146	54	0
Pt0.6/Siral 40	0.60	67	39	0	156	56	0
Pt1.2/Siral 40	1.20	62	43	0	127	42	0
Siral 1	0	0	0	0	163	98	33
Pt0.33/Siral 1	0.33	0	0	0	133	82	17

active than the catalysts based on Siral 40, and that the activity of Pt/Siral 40 catalysts increases with increasing platinum loading.

Due to the sequential reaction steps involved in the isomerization and cracking reactions, product selectivity depends strongly on total conversion. According to the classical bifunctional mechanism, mono-branched feed isomers dominate at low conversion, di- (and multi-) branched isomers start to appear at increasing conversion, while cracking products become significant only at high total conversion [4]. Fig. 3 shows selectivity/conversion plots for the main product lumps on the Pt/Siral 40 catalysts. Although the general trend of increasing selectivity to cracking products and decreasing selectivity to mono-branched feed isomers is followed, a marked difference is noticeable between the catalysts; the selectivity to cracking products at low conversion increases consistently with the platinum loading. The classical bifunctional mechanism alone cannot account for these selectivity/conversion patterns. The increasing cracking selectivity with increasing platinum content is therefore an indication that cracking products are also directly formed from *n*-hexadecane via a parallel hydrogenolytic route.

Carbon-based cracking selectivity curves are represented in Fig. 4. The cracking selectivity of Pt/Siral 1 and a Pd/Siral 40 catalyst with negligible hydrogenolytic activity [26] are reported for

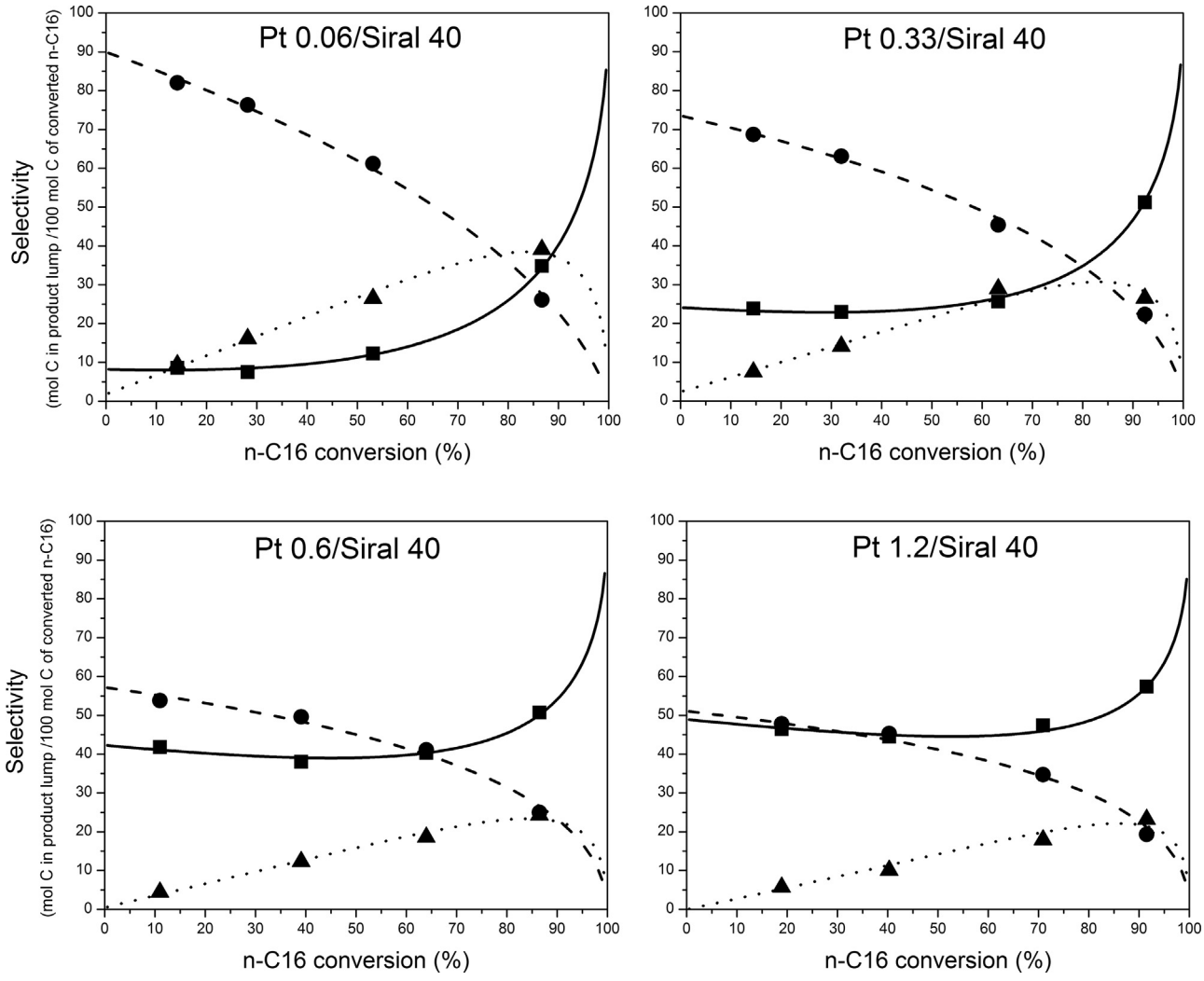

Fig. 3. Selectivity/conversion plots for the Pt/Siral 40 catalysts for the product lumps: mono-branched hexadecanes (- -●- -); multi-branched hexadecanes (··· ▲ ···); cracking products (—■—). Conditions: 310 °C, 30 bar, $H_2/n\text{-}C_{16}H_{34}$ = 10 mol/mol, WHSV = 0.75–18 h^{-1}.

Table 4
First-order rate constants and linear fitting parameters.

Catalyst	Pt loading (wt%)	k_{tot} (h^{-1})	k_{hyd} (h^{-1})	R^2	Intercept
Pt0.06/Siral 40	0.06	2.23 ± 0.12	0.18	0.9985	0.0508
Pt0.33/Siral 40	0.33	2.77 ± 0.16	0.66	0.9964	0.0548
Pt0.6/Siral 40	0.60	3.26 ± 0.23	1.38	0.9991	0.0440
Pt1.2/Siral 40	1.20	3.70 ± 0.059	1.81	1.0000	−0.0013
Pt0.33/Siral 1	0.33	0.0682 ± 0.0058	0.068	0.9908	0.0116

comparison. All the Pt-containing catalysts show non-zero selectivity at zero conversion; this value increases with increasing Pt loading, ranging from ca. 8% for a Pt loading of 0.06-wt% to almost 50% for the catalyst containing 1.2-wt% of platinum. Moreover, the Pt/Siral 1 catalyst shows almost total selectivity to cracking products, while the Pd/Siral 40 catalyst shows the typical pattern of bifunctional hydrocracking. The ratio between cracking and isomerization selectivities at zero-conversion is a measure of the relative importance of the two hydrocracking routes [13,22,36]. Assuming that the decomposition of *n*-hexadecane can follow either a bifunctional route or a "direct cracking" route, and that cracking products at low conversion arise exclusively from direct cracking by hydrogenolysis, the overall rate constant can be proportionally divided in the rate constants for each route, based on their relative selectivities extrapolated to zero-conversion. A further approximation has been made by which monofunctional hydrogenolysis gives rise only to cracking products. Although platinum is known to be active for alkane isomerization, its contribution to the bifunctional route is not significant, as stated by Sinfelt [37]. This assumption is supported by the observation that the selectivity to cracking products on the "monofunctional" catalyst is very close to 90% (Fig. 4).

The total (k_{tot}), bifunctional (k_{bif}) and hydrogenolytic (k_{hyd}) first-order rate constants are plotted against the metal/acid site ratio in Fig. 5. The metal/acid site ratio was calculated dividing the platinum surface area (in m^2/g_{cat}) by the concentration of BAS after desorption of pyridine at 250 °C (in $\mu mol/g_{cat}$). Total hydroconversion activity increases linearly, as does the hydrogenolytic activity, while the bifunctional rate constant is approximately independent of the metal/acid site ratio. This seemingly straightforward result is in contrast to the usual pattern observed for Pt/zeolite catalysts, where hydroconversion activity increases linearly up to the specific metal/acid site ratio corresponding to ideal hydrocracking conditions, after which a plateau is reached [12]. The explanation lies in the fact that the increasing activity is due to monofunctional hydrogenolysis occurring on metal sites alone, when excess metal is present, as was originally observed by Myers and Munns [38] and reported by Weisz [2]. Due to the lower acidity of silica–alumina compared to zeolites, the rate of transformation of intermediate alkenes on the tested Pt/Siral 40 catalysts is expected to be slower; the number of platinum sites necessary to reach ideal hydrocracking conditions is therefore lower. In fact, metal sites seems to be present in excess at a loading as low as 0.06 wt%, where the contribution of Pt-catalyzed hydrogenolysis is already 8% of the total rate.

It is possible, in principle, that the induced acidity caused by the addition of Pt on silica–alumina, is responsible for the observed increase in activity, as speculated by Beuther and Larson [39], who questioned Weisz' hypothesis of monofunctional hydrogenolysis. This effect is taken into account by relating hydroconversion activity to the ratio between the two types of active sites. Anyhow, no correlation could be observed between catalytic activity and the measured Brønsted acidity, whereas a linear correlation was found with metal surface area. This shows that the effect of change in acidity can be neglected in comparison to the added activity due to metal-catalyzed hydrogenolysis.

The total hydroconversion activity on Pt0.33/Siral 1 is much lower than that on the Pt0.33/Siral 40 catalyst. The two catalysts have the same nominal loading of Pt and similar metal surface area. The only property that is greatly different is the Brønsted acidity, responsible for the bifunctional hydrocracking mechanism. If the

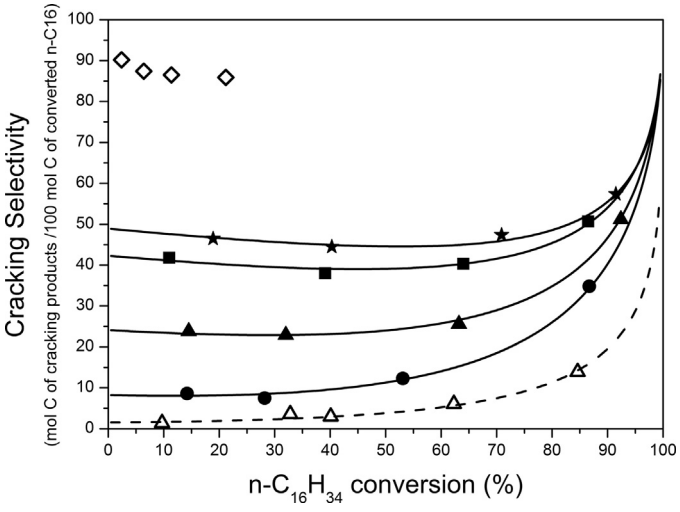

Fig. 4. Cracking selectivity/conversion plots. Pt0.06/S40 (●), Pt0.33/S40 (▲), Pt0.6/S40 (■), Pt1.2/S40 (★), Pt0.33/S1 (◊). Conditions: 310 °C, 30 bar, H_2/*n*-$C_{16}H_{34}$ = 10 mol/mol, WHSV = 0.75–18 h^{-1}. Data obtained on a purely bifunctional 0.33-wt% Pd on Siral 40 (△) are reported for comparison [26].

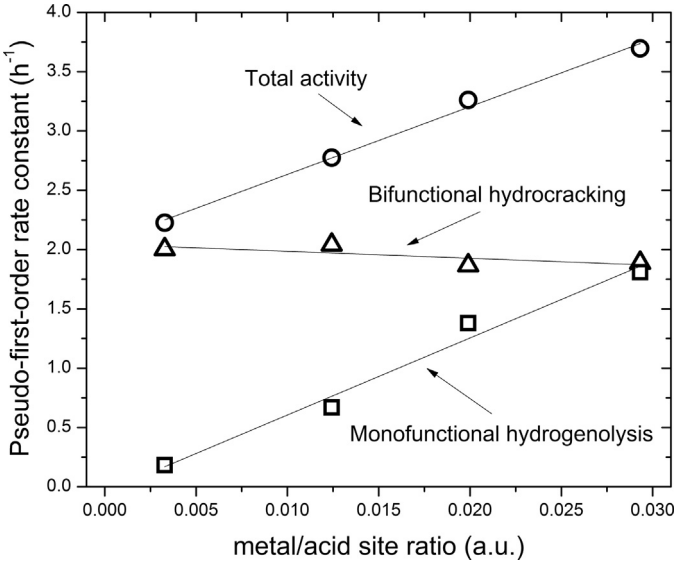

Fig. 5. Hydroconversion activity vs. metal/acid site ratio for the Pt/Siral 40 catalysts. Conditions: 310 °C, 30 bar, H_2/*n*-$C_{16}H_{34}$ = 10 mol/mol, WHSV = 0.75–18 h^{-1}. The values of k_{tot} (○), k_{bif} (△) and k_{hyd} (□) are mean values of the apparent first-order rate constants calculated at different WHSV. Platinum surface area and BAS concentration after desorption of pyridine at 250 °C were used in calculating the metal/acid site ratios.

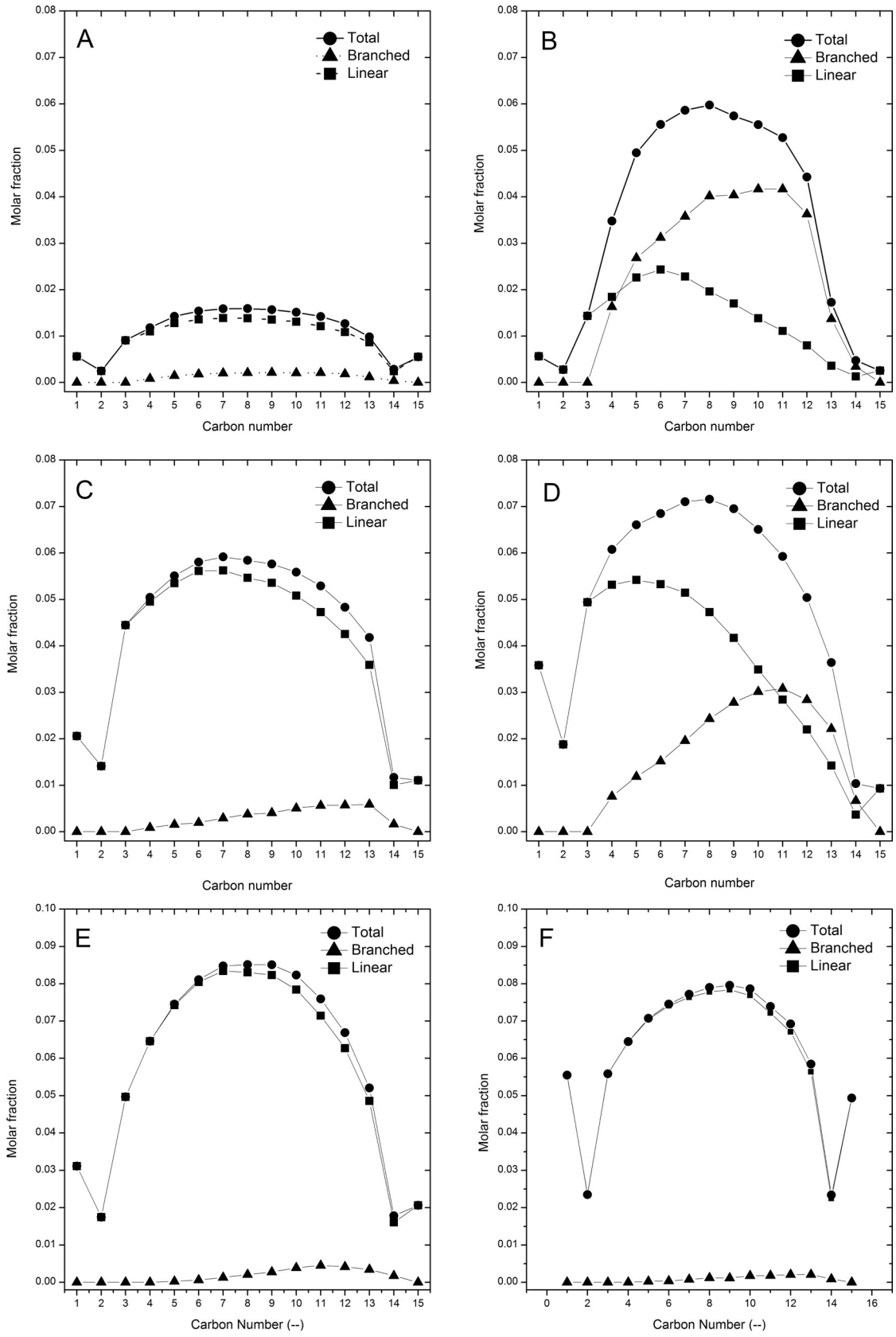

Fig. 6. Cracking product distribution on: (A) Pt0.06/Siral 40, n-$C_{16}H_{34}$ conversion = 14.2%; (B) Pt0.06/Siral 40, n-$C_{16}H_{34}$ conversion = 86.7%; (C) Pt1.2/Siral 40, n-$C_{16}H_{34}$ conversion = 18.9%; (D) Pt1.2/Siral 40, n-$C_{16}H_{34}$ conversion = 91.5%; (E) Pt1.2/Siral 40 during addition of pyridine, n-$C_{16}H_{34}$ conversion = 6.0%; (F) Pt 0.33/Siral 1, n-$C_{16}H_{34}$ conversion = 6.5%.

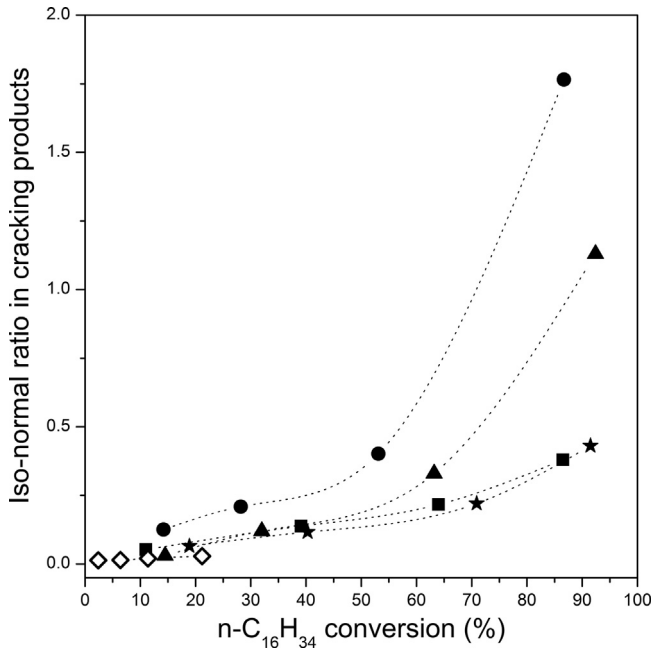

Fig. 7. Iso-to-normal paraffin ratio in the cracking products as a function of *n*-hexadecane conversion for Pt0.06/S40 (●), Pt0.33/S40 (▲), Pt0.6/S40 (■), Pt1.2/S40 (★), Pt0.33/S1 (◊). Conditions: 310 °C, 30 bar, $H_2/n\text{-}C_{16}H_{34}$ = 10 mol/mol, WHSV = 0.75–18 h^{-1}. The lines are eye guides only.

speculations about the added hydrogenolytic activity of the Pt sites are correct, we expect that the total activity of the Pt0.33/Siral 1 catalyst would be similar to the hydrogenolytic activity on Pt0.33/Siral 40, i.e. similar specific rates on platinum sites. The rate values reported in Table 4 show that this is not the case: The rate constant for hydrogenolysis on the non-acidic catalyst (Pt0.33/Siral 1) is one order of magnitude lower. Consequently, it could be argued that either the hydrogenolytic activity on Pt0.33/Siral 40 is not only due to the platinum sites, or that their monofunctional catalytic activity depends on the support.

3.2.2. Distribution of cracking products

Distributions of cracking products obtained on two of the Pt/Siral 40 catalysts at high and low total conversion are shown in Fig. 6. Symmetric carbon-number distributions were typically observed, with a slight contribution of secondary cracking at high conversions; the typical ratios between moles of cracking products and moles of cracked *n*-hexadecane were within 2 and 2.1. Remarkable differences were observed in the content of branched isomers. The ratio between branched and normal paraffins (iso/normal ratio) increased with increasing total conversion and with decreasing Pt loading. The dependence on conversion is expected in a bifunctional hydrocracking scheme, where the increasing population of multi-branched isomers promotes the occurrence of Type A β-scission, which gives rise to two branched fragments [40]. The iso/normal ratio is also dependent on the Pt loading, decreasing markedly with increasing amount of platinum on the catalyst (Fig. 7). At high total conversion (ca. 85%) a difference larger than factor four is observed between the Pt0.06/Siral 40 and the Pt0.6/Siral 40 (1.76 vs. 0.37). This follows naturally from the hypothesis of the increasing importance of the hydrogenolysis mechanism, which produces only linear fragments.

3.2.3. Methane selectivity on acid and non-acid catalysts

Methane can only be formed through the hydrogenolytic pathway. The high instability of primary carbenium ions makes methane formation through Type D β-scission very unfavorable

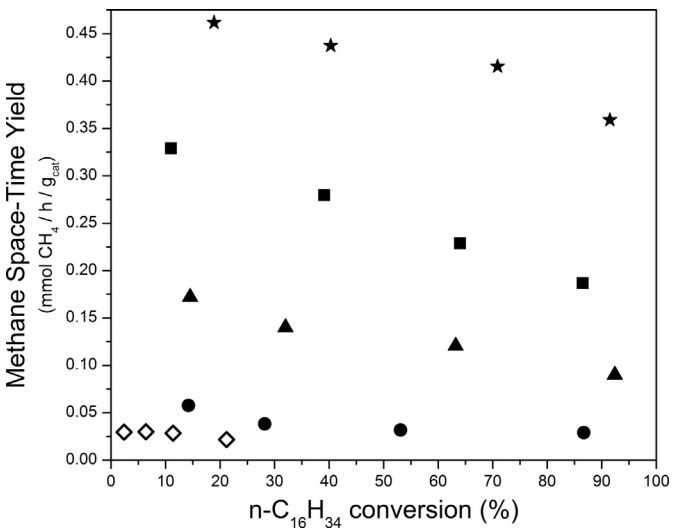

Fig. 8. Space–time yield of methane as a function of *n*-hexadecane conversion for Pt0.06/S40 (●), Pt0.33/S40 (▲), Pt0.6/S40 (■), Pt1.2/S40 (★), Pt0.33/S1 (◊). Conditions: 310 °C, 30 bar, $H_2/n\text{-}C_{16}H_{34}$ = 10 mol/mol, WHSV = 0.75–18 h^{-1}.

[40]. The rate of formation of methane can therefore be used for discriminating between the two hydrocracking routes. The space–time yield (STY, defined as millimoles produced per unit mass of catalyst per unit time) of methane is plotted versus total conversion in Fig. 8. A strong dependence both on Pt content and conversion can be observed: methane yield increases with increasing loading and decreases with increasing total conversion.

The dependence on conversion of the methane STY can be compared with that of mono-branched hexadecanes (Fig. 9), which are primary products generated from the bifunctional route. The isomer yield decreases linearly with total conversion, but shows no dependence on Pt loading. This is further indication that isomerization products are formed by acid-catalyzed reactions whose rate is not limited by the reaction steps occurring on the metal sites. The effect of conversion on methane yield can be explained by two concurring factors: At high conversion the contribution of the bifunctional mechanism increases, increasing the concentration of isomerized species, which are prone to undergo acid-catalyzed

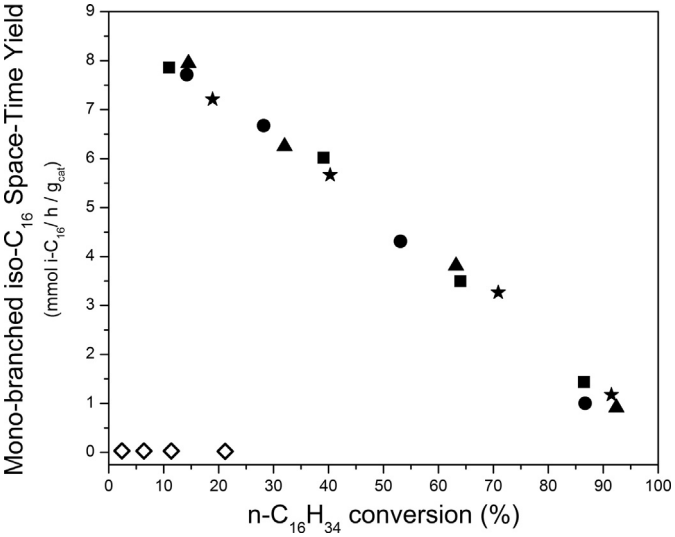

Fig. 9. Space–time yield of mono-branched hexadecanes as a function of *n*-hexadecane conversion for Pt0.06/S40 (●), Pt0.33/S40 (▲), Pt0.6/S40 (■), Pt1.2/S40 (★), Pt0.33/S1 (◊). Conditions: 310 °C, 30 bar, $H_2/n\text{-}C_{16}H_{34}$ = 10 mol/mol, WHSV = 0.75–18 h^{-1}.

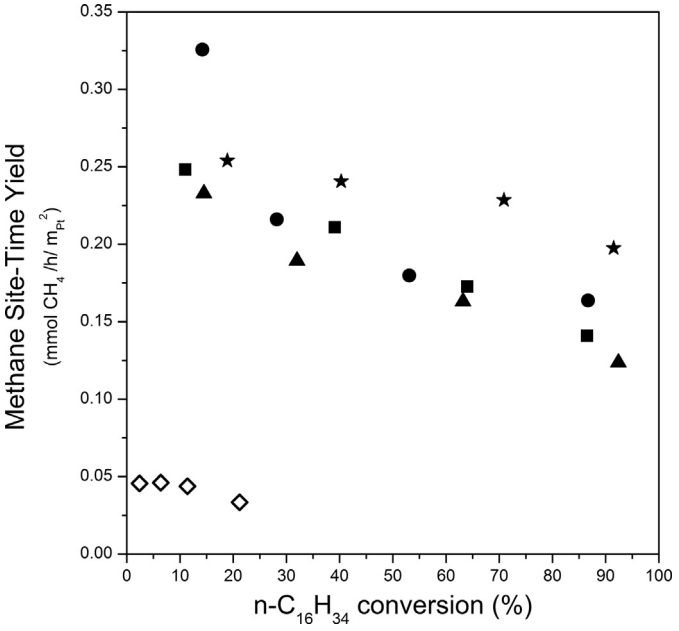

Fig. 10. Specific methane yield per Pt surface area as a function of *n*-hexadecane conversion. Pt0.06/S40 (●), Pt0.33/S40 (▲), Pt0.6/S40 (■), Pt1.2/S40 (★), Pt0.33/S1 (◊). Conditions: 310 °C, 30 bar, H_2/*n*-$C_{16}H_{34}$ = 10 mol/mol, WHSV = 0.75–18 h^{-1}.

cracking by the fast modes of β-scission [40] and are therefore less readily demethylated on the metal sites. The higher conversion will also increase the concentration of olefinic intermediates, which will compete for adsorption on metal sites. The methane STY is very low on Pt0.33/Siral 1, despite its metal surface area being comparable with that of the Pt0.33/Siral 40 catalyst.

The methane yield can be recalculated as a site-time yield, defined as millimoles produced per unit Pt surface area per unit time. The site-time yields for the tested catalysts are shown in Fig. 10. If methane is produced only by hydrogenolysis occurring exclusively by metal catalysis, no variations of the specific yield on the different catalysts should be observed, except for possible effects of metal crystallite size. Site-time yields fall indeed in a narrow range on the Pt/Siral 40 catalysts, except for the slightly higher values observed for Pt1.2/Siral 40. This deviation, particularly apparent at higher conversion, can be ascribed to secondary demethylation, occurring to some extent on the catalyst with highest Pt loading, as can be seen by the higher fraction of methane in the cracking products distribution (Fig. 6D). A major deviation is the much lower methane site-time yield on the non-acid catalyst, with values below 0.05 mmol/h/m^2, which is lower by a factor five compared to the Siral 40-based catalysts.

This observation either implies that Brønsted acid sites participate in the hydrogenolytic mechanism, or that Pt sites supported on the Siral 40 material are intrinsically more active for hydrogenolysis. Since particle size and dispersion are quite similar for the Pt0.33/Siral 1 and the Pt0.33/Siral 40 catalysts, the reason for the different activity have to be found in other properties of the metal crystallites. It is generally known that metal-support interactions affect the activity of metal catalysts in hydrogenation and hydrogenolysis reactions, but the underlying reasons are debated. The increased activity for benzene hydrogenation of Pt supported on acid supports was ascribed to adsorption of reaction intermediates in the metal–acid interfacial region, which then reacted with spilt-over hydrogen from Pt sites [41]; Lercher and coworkers explained the higher turnover frequency of Pt/ASA catalysts for neopentane hydrogenolysis with the increasing electronegativity of the support, increasing the electron deficiency of Pt sites, causing a stronger adsorption of the reactant [33]. Koningsberger et al. singled out the role of hydrogen coverage, which decreased with increasing acidity of the support; neopentane adsorbed more strongly at lower hydrogen coverage [42]. Another study proposed that the role of Brønsted acid sites was to form protonated palladium species which were highly active in the conversion of neopentane [43].

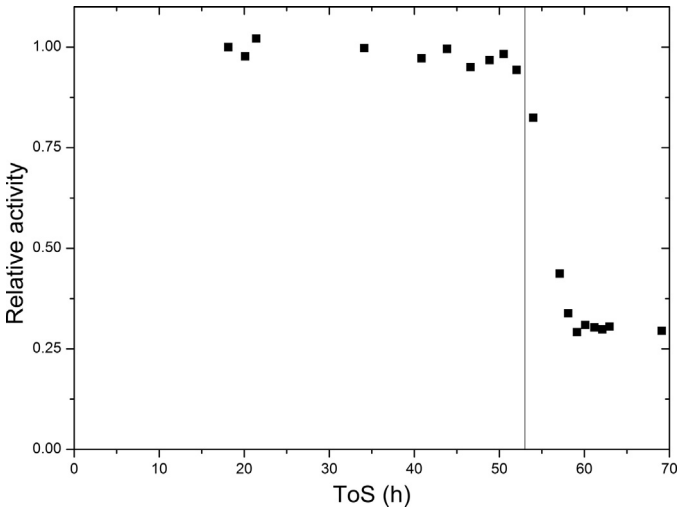

Fig. 11. Activity drop during the co-feeding of pyridine on Pt1.2/S40. Conditions: 310 °C, 30 bar, H_2/*n*-$C_{16}H_{34}$ = 10 mol/mol, WHSV = 0.75–18 h^{-1}.

In the light of our results, it seems that direct hydrogenolysis of *n*-alkanes on Pt sites might be affected by interactions between the metal particles and the support in a similar manner as that observed for neopentane hydrogenolysis. To gather more proof that this behavior is not due to mechanistic involvement of Brønsted sites, but rather to intrinsic catalytic properties of the metal particles, selective poisoning of acid sites on a Pt/Siral 40 catalyst was performed.

3.2.4. *Effect of hydrogen pressure and selective poisoning of acid sites*

When the effects of metal–acid interactions on hydrogenolysis reactions are studied, care must be taken to avoid introducing bifunctional reactions which might influence alkane hydroconversion in the presence of acidity. Neopentane is generally used as it cannot form alkene intermediates, necessary for the bifunctional hydrocracking mechanism [42]. For the investigation of similar effects on the hydrogenolysis of linear alkanes, a way of inhibiting bifunctional activity is to selectively poison the acid sites with a base such as pyridine [44,45]. This approach allows for the qualitative study of monofunctional, metal-catalyzed reactions in the presence of an acid support.

Pyridine was therefore co-fed with *n*-hexadecane on a 1.2-wt% Pt/Siral 40 catalyst with stable activity. The effect of pyridine was immediately noticeable: After one hour of co-feeding, no branched hydrocarbons could be detected in the gaseous products. The total catalytic activity dropped considerably and stabilized after a few hours (Fig. 11). After that, experiments at varying hydrogen partial pressures were performed.

Pyridine decomposed into *n*-pentane and ammonia on the Pt1.2/Siral 40 catalyst. The conversion of pyridine, calculated by the added amount of *n*-pentane observed on top of the typical cracking products distribution, was approximately 50%. Decomposition of pyridine occurs most probably on Pt sites, through piperidine and 1-pentylamine, by hydrogenation of double bonds followed by hydrodenitrogenation [46]. This is, of course, a drawback for the determination of the absolute hydrogenolytic activity of the metal sites. Nevertheless, a qualitative analysis can still be of interest. The

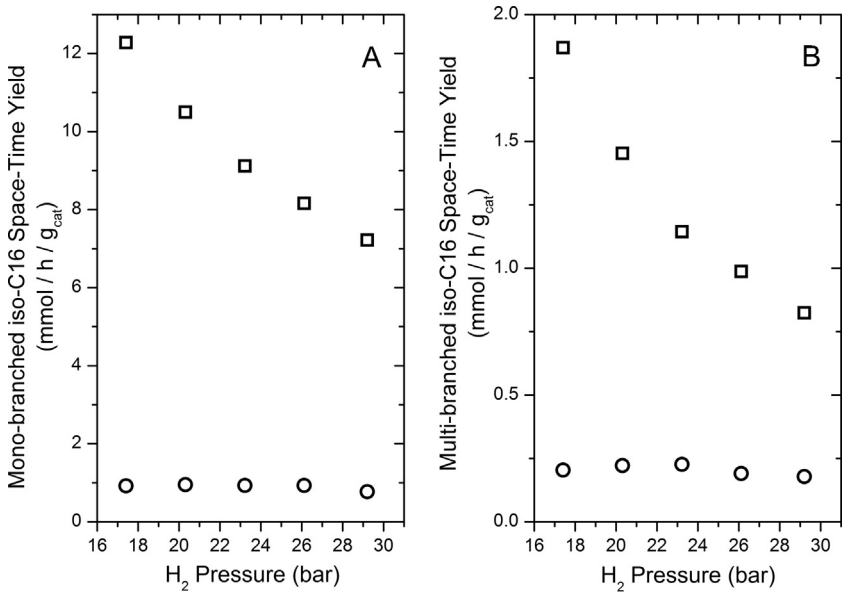

Fig. 12. Space–time yield of mono-branched (A) and multi-branched hexadecanes (B) as a function of hydrogen partial pressure before (□) and during (○) the addition of pyridine. Catalyst: Pt1.2/S40. Conditions: 310 °C, 30 bar, H_2/n-$C_{16}H_{34}$ = 6–10 mol/mol, WHSV = 18 h^{-1}.

fact that space–time yields of branched hexadecanes (Fig. 12) are reduced by one order of magnitude, while yields to methane and normal alkanes (Fig. 13) are much less affected, shows that pyridine blocks the hydroisomerization/cracking function of the acid sites.

The distribution of cracking products on a Pt/Siral 40 catalyst during addition of pyridine (Fig. 6E) can be compared with that obtained on the non-acidic Pt/Siral 1 catalyst (Fig. 6F). In both case the isomer content is very low and the only difference is in the relative amounts of C1 and C15, which are higher on the non-acidic catalyst. This implies that the rate of terminal vs. internal bond hydrogenolysis is relatively lower on the pyridine-poisoned Pt1.2/Siral 40 catalyst.

The results of the study on the effect of the partial pressure of hydrogen are reported in a comparative way. The same conditions of total pressure, temperature and flow rates were used in absence and presence of pyridine. Considering the large excess of hydrogen, its partial pressure can be assumed constant throughout the reactor. Moreover, *n*-hexadecane conversion levels were quite low (<20%); the use of inlet hydrogen pressure and of space–time yields instead of rates is therefore justified.

It is known that, for ideal hydrocracking conditions, hydrogen partial pressure changes the equilibrium of the alkane dehydrogenation reaction. At constant alkane concentration, lower hydrogen pressures cause a proportional increase of the steady

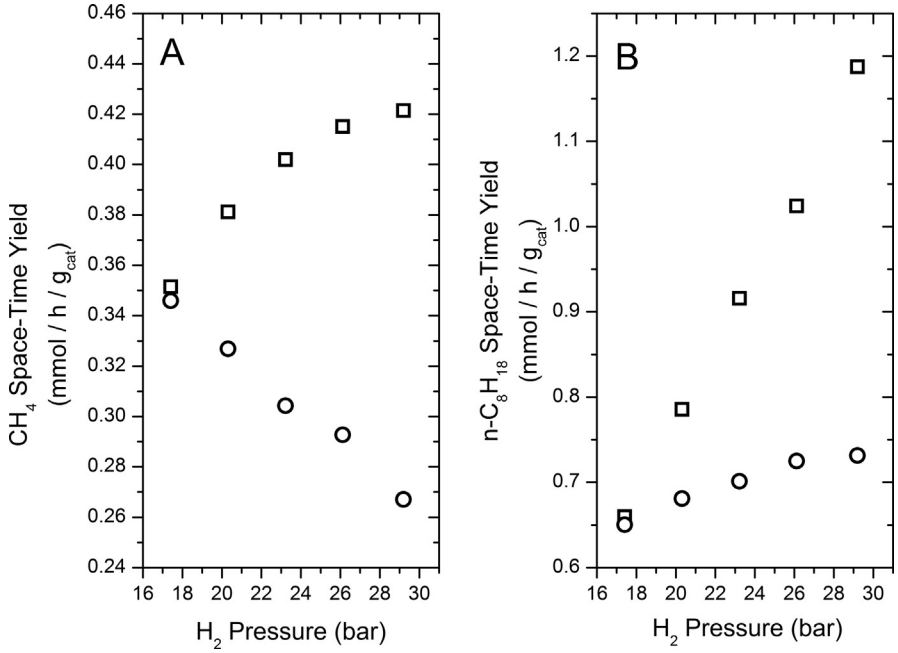

Fig. 13. Space–time yield of methane (A) and *n*-octane (B) as a function of hydrogen partial pressure before (□) and during (○) the addition of pyridine. Catalyst: Pt1.2/S40. Conditions: 310 °C, 30 bar, H_2/n-$C_{16}H_{34}$ = 6–10 mol/mol, WHSV = 18 h^{-1}.

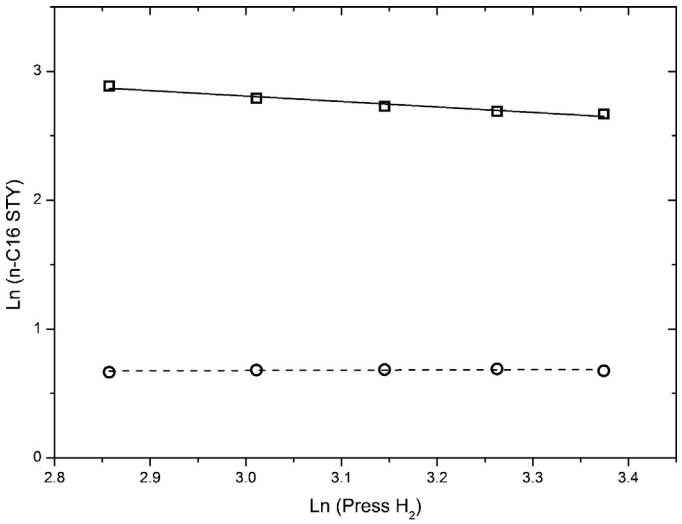

Fig. 14. Bi-logarithmic plot of the overall reaction rate as a function of hydrogen partial pressure before (□) and during (○) the addition of pyridine. Catalyst: Pt1.2/S40. Conditions: 310 °C, 30 bar, H_2/*n*-$C_{16}H_{34}$ = 6–10 mol/mol, WHSV = 18 h^{-1}.

state concentration of the olefins formed on the metal sites, which subsequently react on the acid sites. Its influence on the overall rate is thermodynamic rather than kinetic. According to this scheme the apparent reaction order for hydrogen under ideal hydrocracking conditions is expected to be −1, as indeed reported in the literature [21,22]. In Fig. 14 the bi-logarithmic plot of the total rate against hydrogen partial pressure is shown. The reaction order for hydrogen was calculated by linear regression, and resulted to be −0.42 on the non-poisoned catalyst. This discrepancy with literature data is probably due to the high contribution of hydrogenolysis on the total rate. In the presence of pyridine, the overall reaction rate seems to be unaffected by hydrogen pressure (apparent reaction order = 0.05). As can be seen in Fig. 12, the isomerization rate is affected in a similar way: negative order at reference conditions (reaction order = −1.0) and little or no influence of hydrogen pressure in the presence of pyridine. These facts are further indications that acid-catalyzed reactions are indeed inhibited by pyridine.

Fig. 13A and B shows the dependence on hydrogen pressure of the rates of formation of methane and *n*-octane, respectively. It can be noted that the absolute values of space–time yields are of the same order of magnitude with and without addition of pyridine, indication that hydrogenolytic reactions are much less affected by the presence of pyridine compared to the acid-catalyzed reactions. At reference conditions, the effect of hydrogen partial pressure is positive for both the rate to methane and the rate to other cracking products. The latter shows first-order dependence while a less marked positive influence is observed on methane formation (apparent reaction order: 0.35). In the presence of pyridine, hydrogen pressure has a positive effect on the space–time yield to metal-catalyzed hydrogenolysis products, while the rate to methane shows a negative order in hydrogen.

Hydrogenolysis is usually reported to have a first-order dependence on alkane concentration and negative dependence on hydrogen pressure [47]. However, the situation in our case is complicated by the presence of bifunctional activity, the equilibrium of dehydrogenation/hydrogenation reactions, and the reactions of pyridine decomposition on the metal sites. This catalytic and reaction system is not suitable for detailed kinetic analyses of the mechanisms involved, and such were outside the scope of this work.

Nevertheless, the monofunctional pathway appears to proceed ten times faster on platinum sites if these are supported on a silica–alumina with Brønsted and Lewis acidity, compared to platinum sites supported on a silica–alumina of comparable Lewis acidity but negligible Brønsted acidity.

4. Conclusions

A series of catalysts consisting of platinum on silica–aluminas were tested in the hydroconversion of *n*-hexadecane. The effect of platinum loading on the acid properties of the catalysts and on their catalytic activity and selectivity was investigated. Total hydroconversion activity showed a linear increase with platinum loading.

The bifunctional hydrocracking pathway showed constant reaction rates at platinum loadings ranging between 0.06 and 1.2 wt%, and the observed increase in activity could be related to a hydrogenolytic pathway yielding normal alkanes, including methane and ethane. The yield of methane, as well as the yield of linear hydrocarbons at low *n*-hexadecane conversion could be linearly related to platinum surface area on catalysts with similar acidic properties and platinum dispersion, showing that hydrogenolysis is purely metal catalyzed.

Addition of platinum was found to impact on the acidic properties of the catalysts, increasing the concentration of weak Brønsted and Lewis acid sites. Conversely, support acidity strongly influenced the catalytic properties of platinum crystallites. High hydrogenolytic activity was observed on catalysts containing Brønsted acidity. A catalyst with similar metal dispersion, but using a support of negligible Brønsted acidity, presented rates of hydrogenolysis one order of magnitude lower.

Selective poisoning of acid sites of a Pt/silica-alumina catalyst was performed. Bifunctional activity was successfully suppressed, while hydrogenolysis rates were less affected by the presence of pyridine. This indicates that the role of acidity in the hydrogenolysis reactions is related to changes induced on the platinum sites, probably by charge transfer from the metal particle to the framework atoms of the support, and not to the involvement of acid sites in the mechanism.

Acknowledgments

Atte Aho, Process Chemistry Centre, Åbo Akademi University is kindly acknowledged for the pyridine adsorption measurements. The authors wish to thank Rodrigo Suárez París and Matteo Lualdi for fruitful discussion and Christina Hörnell for improving the English language of this paper. The Swedish Energy Agency is acknowledged for financial support and Sasol Germany GmbH for providing the silica–alumina materials.

References

[1] H.L. Coonradt, W.E. Garwood, Ind. Eng. Chem. Process Des. Dev. 3 (1964) 38–45.
[2] P.B. Weisz, Adv. Catal. 13 (1962) 137–190.
[3] J. Weitkamp, Prepr.—Am. Chem. Soc., Div. Pet. Chem. 20 (1975) 489–507.
[4] C. Bouchy, G. Hastoy, E. Guillon, J.A. Martens, Oil Gas Sci. Technol. Rev. IFP 64 (2009) 91–112.
[5] J. Weitkamp, ChemCatChem 4 (2012) 292–306.
[6] P.N. Kuznetsov, J. Catal. 218 (2003) 12–23.
[7] J.L. Carter, J.A. Cusumano, J.H. Sinfelt, J. Catal. 20 (1971) 223–229.
[8] G.C. Bond, Platinum Met. Rev. 19 (1975) 126–134.
[9] P. Gallezot, in: B. Imelik, C. Naccache, Y.B. Taarit, J.C. Vedrine, G. Coudurier, H. Praliaud (Eds.) Stud. Surf. Sci. Catal. 5 (1980) 227–234.
[10] M. Boudart, Adv. Catal. 20 (1969) 153–166.
[11] O.A. Larson, D.S. MacIver, H.H. Tobin, R.A. Flinn, Ind. Eng. Chem. Process Des. Dev. 1 (1962) 300–305.
[12] F. Alvarez, F.R. Ribeiro, G. Perot, C. Thomazeau, M. Guisnet, J. Catal. 162 (1996) 179–189.
[13] M.J. Girgis, Y.P. Tsao, Ind. Eng. Chem. Res. 35 (1996) 386–396.
[14] R. Ravishankar, S. Sivasanker, Appl. Catal., A 142 (1996) 47–59.
[15] F. Ribeiro, C. Marcilly, M. Guisnet, J. Catal. 78 (1982) 267–274.
[16] M. Guisnet, F. Alvarez, G. Giannetto, G. Perot, Catal. Today 1 (1987) 415–433.

[17] T.F. Degnan, C.R. Kennedy, AIChE J. 39 (1993) 607–614.
[18] V. Calemma, S. Peratello, S. Pavoni, G. Clerici, C. Perego, in: E. Iglesia, J.J. Spivey, T.H. Fleisch (Eds.) Stud. Surf. Sci. Catal. 136 (2001) 307–312.
[19] D. Leckel, Ind. Eng. Chem. Res. 46 (2007) 3505–3512.
[20] J. Kang, W. Ma, R.A. Keogh, W.D. Shafer, G. Jacobs, B.H. Davis, Catal. Lett. 142 (2012) 1295–1305.
[21] I. Rossetti, C. Gambaro, V. Calemma, Chem. Eng. J. 154 (2009) 295–301.
[22] V. Calemma, S. Peratello, C. Perego, Appl. Catal., A 190 (2000) 207–218.
[23] E. Blomsma, J.A. Martens, P.A. Jacobs, in: H. Chon, S.-K. Ihm, U. Young Sun (Eds.) Stud. Surf. Sci. Catal. 105 (1997) 909–916.
[24] W. Böhringer, A. Kotsiopoulos, M. de Boer, C. Knottenbelt, J.C.Q. Fletcher, in: B.H. Davis, M.L. Occelli (Eds.) Stud. Surf. Sci. Catal. 163 (2007) 345–365.
[25] C.A. Emeis, J. Catal. 141 (1993) 347–354.
[26] F. Regali, M. Boutonnet, S. Järås, Catal. Today 214 (2013) 12–18.
[27] B.J. Kip, F.B.M. Duivenvoorden, D.C. Koningsberger, R. Prins, J. Catal. 105 (1987) 26–38.
[28] W. Daniell, U. Schubert, R. Glöckler, A. Meyer, K. Noweck, H. Knözinger, Appl. Catal., A 196 (2000) 247–260.
[29] E. Peeters, M. Cattenot, C. Geantet, M. Breysse, J.L. Zotin, Catal. Today 133–135 (2008) 299–304.
[30] I.S. Pieta, M. Ishaq, R.P.K. Wells, J.A. Anderson, Appl. Catal., A 390 (2010) 127–134.
[31] M.F. Williams, B. Fonfé, C. Sievers, A. Abraham, J.A. van Bokhoven, A. Jentys, J.A.R. van Veen, J.A. Lercher, J. Catal. 251 (2007) 485–496.
[32] D.C. Koningsberger, M.K. Oudenhuijzen, D.E. Ramaker, J.T. Miller, in: A. Corma, F.V. Melo, S. Mendioroz, J.L.G. Fierro (Eds.) Stud. Surf. Sci. Catal. 130 A (2000) 317–322.
[33] M.F. Williams, B. Fonfé, C. Woltz, A. Jentys, J.A.R. van Veen, J.A. Lercher, J. Catal. 251 (2007) 497–506.
[34] D. Kubička, N. Kumar, T. Venäläinen, H. Karhu, I. Kubičková, H. Österholm, D.Y. Murzin, J. Phys. Chem. B 110 (2006) 4937–4946.
[35] D. Santi, S. Rabl, V. Calemma, M. Dyballa, M. Hunger, J. Weitkamp, ChemCatChem 5 (2013) 1524–1530.
[36] N.A. Bhore, M.T. Klein, K.B. Bischoff, Ind. Eng. Chem. Res. 29 (1990) 313–316.
[37] J.H. Sinfelt, Adv. Catal. 23 (1973) 91–119.
[38] C.G. Myers, G.W. Munns, Ind. Eng. Chem. 50 (1958) 1727–1732.
[39] H. Beuther, O.A. Larson, Ind. Eng. Chem. Process Des. Dev. 4 (1965) 177–181.
[40] J. Weitkamp, P.A. Jacobs, J.A. Martens, Appl. Catal. 8 (1983) 123–141.
[41] S.D. Lin, M.A. Vannice, J. Catal. 143 (1993) 539–553.
[42] D.C. Koningsberger, M.K. Oudenhuijzen, J. de Graaf, J.A. van Bokhoven, D.E. Ramaker, J. Catal. 216 (2003) 178–191.
[43] S.T. Homeyer, Z. Karpiński, W.M.H. Sachtler, J. Catal. 123 (1990) 60–73.
[44] K.H.W. Robschlager, C.A. Emeis, R.A. van Santen, J. Catal. 86 (1984) 1–8.
[45] G. Larsen, L.M. Petkovic, Appl. Catal., A 148 (1996) 155–166.
[46] Z. Vít, M. Zdražil, J. Catal. 119 (1989) 1–7.
[47] G.C. Bond, Metal-Catalysed Reactions of Hydrocarbons, Springer, New York, NY, 2005, pp. 525–589.